Rheologica Acta (2021) 60:263–276
https://doi.org/10.1007/s00397-021-01269-1

ORIGINAL CONTRIBUTION

Enhanced magnetorheological effect of suspensions based on carbonyl iron particles coated with poly(amidoamine) dendrons

Tomas Plachy[1,2] · Martin Cvek[1] · Lukas Munster[1] · Barbora Hanulikova[1] · Pavol Suly[1] · Alenka Vesel[3] · Qilin Cheng[1,2]

Received: 1 October 2020 / Revised: 16 March 2021 / Accepted: 23 March 2021 / Published online: 5 April 2021

Abstract

Particle oxidation constitutes a serious ageing phenomenon in magnetorheological suspensions, bringing about deterioration in performance. This study describes commercial carbonyl iron particles that were successfully coated with poly(amidoamine) dendrons and then applied as an oxidation-resistant dispersed phase in magnetorheological suspensions. A synthesis method was adhered to whereby the particles were sequentially treated with ethylenediamine and methyl acrylate, leading to the formation of generation 2 and 2.5 dendrons; these had the capacity for composite particles with a nano-scale dendritic layer to be prepared on their surfaces. Success in applying the coating was confirmed by various techniques, including XPS, TEM, EDX, FTIR and Raman spectroscopy. The controlled approach adopted to coating the carbonyl iron particles resulted in them exhibiting sufficient oxidation stability, with only an ~ 4.5–4.7% decrease in saturation magnetization. Of interest was that their magnetorheological suspensions demonstrated ca 4.8% and 4% higher dynamic yield stress than a suspension based on non-modified particles at the highest intensity of magnetic field investigated, i.e. 438 kA m^{-1}. Notably, sedimentation stability was evaluated by a unique method that involved the use of a tensiometer with a specific testing probe. The aforementioned coating process led to enhanced sedimentation stability of the magnetorheological suspensions based on coated particles possibly due to decrease in the overall density of the particles, enhanced dispersion stability and reduction in the size of their agglomerates in the silicone oil mixtures that were confirmed by optical microscopy. Modification of the particles as proposed has the potential to overcome one of the primary drawbacks of magnetorheological suspensions, this being oxidation instability (which leads to what is referred to as "in-use-thickening"), without negatively affecting their performance in the presence of a magnetic field.

Keywords Carbonyl iron · Magnetorheology · Yield stress · Sedimentation stability · Poly(amidoamine)

Introduction

Magnetorheological (MR) suspensions (MRSs) are intelligent systems whose rheological parameters can be controlled through applying a magnetic field. They are generally composed of a non-magnetic liquid medium and a dispersed phase of magnetic particles, most commonly carbonyl iron particles (CIPs). These otherwise randomly distributed particles create chain-like structures when exposed to a magnetic field (Feijoo et al. 2020; Machovsky et al. 2015; Marins et al. 2019), causing an abrupt rise in viscosity and other rheological parameters of such MRSs (Bell et al. 2008; Bombard et al. 2015; Cvek et al. 2020; De Vicente et al. 2011; Han et al. 2019; Morillas et al. 2018). Behaviour of this type is referred to as the MR effect, which has found numerous industrial applications, including in damping systems, shock absorbers, as a medium in an MR clutch and in MR

✉ Tomas Plachy
plachy@utb.cz

✉ Qilin Cheng
chengql@ecust.edu.cn

[1] Centre of Polymer Systems, University Institute, Tomas Bata University in Zlin, Trida Tomase Bati 5678, 760 01 Zlin, Czech Republic

[2] Key Laboratory for Ultrafine Materials of the Ministry of Education, School of Materials Science and Engineering, East China University of Science and Technology, Shanghai 200237, China

[3] Department of Surface Engineering and Optoelectronics, Jozef Stefan Institute, Jamova cesta 39, 1000 Ljubljana, Slovenia

polishing (Bucchi et al. 2013; Chen et al. 2003; Kwon et al. 2015; Park et al. 2010; Utami et al. 2018; Zhu et al. 2012).

A recognized issue affecting MRSs is that during long-term operation, they undergo what is referred to as "in-use-thickening" (IUT) (Carlson and Jolly 2000; Utami et al. 2018). This brings about increase in the resistive force of the instrument, accompanied by the given system showing rise in yield stress values in the absence of a magnetic field (Roupec and Mazurek 2011; Roupec et al. 2013). In-use-thickening is caused by abrasion or delamination of the oxidized layers on the surfaces of CIPs (Ulicny et al. 2007), constituting a primary drawback of MRSs. For example, Ulicny et al. (2007) utilized an MRS as an operating medium in an MR clutch. During the investigation and simulation of its use, the MRS was exposed to temperatures of up to 250 °C, leading to significant oxidation of the CIPs and increase in the oxygen content on their surfaces, rising from 0.47 to 7 wt%. Indeed, a layer of iron oxide on the surfaces of the CIPs also diminishes rheological parameters in the presence of a magnetic field (Plachy et al. 2018; Ulicny et al. 2007). Even though the MR effect of such a device may only be slightly lessened in some cases (Roupec and Mazurek 2011), IUT dramatically depreciates the properties of MRSs and raises operating demands connected to lower performance and higher power consumption in the absence of a magnetic field, hence is considered an undesirable phenomenon of MRSs (Carlson and Jolly 2000; Roupec and Mazurek 2011).

A potential means of improving the oxidation stability of the particles is to fabricate core–shell particles, wherein the magnetic core is coated with a polymeric or inorganic shell (Cvek et al. 2015b; Han et al. 2018; Park et al. 2015, 2016; Seo et al. 2018; Zhang et al. 2018). Magnetorheological suspensions based on such composite particles have been shown to exhibit a lower coefficient of friction compared to MRSs based on bare particles, as they can lower their general abrasion and extend the service life of an MR device (Zhang, Dong, Choi and Lee 2018). Supplementing a non-magnetic polymeric layer on the surface of CIPs, however, generally leads to decrease in values for saturation magnetization (M_s) (Lee et al. 2017; Machovsky et al. 2014) of the particles; this plays an important role in determining the rheological parameters of an MRS in the presence of a magnetic field. Cvek et al. (2015b) have recently proposed surface-initiated atom transfer radical polymerization (ATRP) as a tool to facilitate a controlled CIP coating process. They demonstrated that the M_s of the core–shell CIPs (CIP–poly(glycidyl methacrylate)) only decreased by about 4% in comparison with bare CIPs. An approach like theirs could result in an MRS with heightened oxidation stability, wherein the M_s of the particles is retained together with enhanced MR effects. Nevertheless, ATRP requires a complex reaction system, usually one containing a copper halide catalyst and amide-based ligand (Matyjaszewski 2012). Removal of the catalyst is considered the main drawback, which alongside the air sensitivity of the reaction hinder general adoption by industry. These reasons explain the motivation to introduce a different method capable of providing complementary results with significant potential for practical application.

The goal of this study is to introduce a novel approach to coating a CIP surface with an organic polymeric layer based on poly(amidoamine) (PAMAM) dendrons with step-by-step synthesis, which enables control over the thickness of the layer. Poly(amidoamine) is a common dendrimer that possesses a globular, monodisperse and highly branched structure (Fréchet and Tomalia 2001). It is prepared by sequential synthesis, facilitating the preparation of dendrimers of various generations (Gx), permitting further definition of properties and size (Demir et al. 2014). For these reasons, it represents a suitable candidate for application as an organic layer on the surface of CIPs in magnetorheology, reducing the agglomeration of particles and concurrently providing chemical and oxidation protection.

Herein, two novel magnetic core–shell particles were prepared, utilizing PAMAM dendrons of generation 2 (G2) and G2.5. This led to formation of a very thin organic layer on the surface of the CIPs, which preserved their level of M_s while also exhibiting enhanced thermal and chemical stability. The MR performance of their MRSs was examined, and dynamic and static yield stress values were estimated. Interestingly, the values for dynamic yield stress were found to be ca 5% higher for the MRSs based on the coated particles than the reference MRS based on carbonyl iron particles.

Materials and methods

Materials and chemicals

Commercial CIPs, grade SL ($d_{50} = 8.5$ µm; with a minimum Fe content of 99.5%), were obtained from BASF (Germany). Ethylenediamine (ED; purity > 99.5%), methyl acrylate (MA; purity > 99%) and potassium bromide (FTIR grade, ≥ 99% trace metals basis) were purchased from Sigma-Aldrich (USA). The methyl acrylate and APTES were utilized in the form as received, while the ED and anhydrous methanol were dried prior to use using layers of sodium or molecular sieves, the latter at a mesh pore size of 0.3 nm. Hydrochloric acid (HCl), ethanol (p.a.), acetone (p.a.) and toluene (purity > 99%) were purchased from Penta Chemicals (Czech Republic). Silicone oil (Lukosiol M200, Chemical Works Kolín, Czech Republic, viscosity $\eta_c = 194$ mPa s at 25 °C) was employed as a medium for preparing the MRSs.

Application of CIP coating with PAMAM dendrons

The surface of the CIPs was initially activated in order to create hydroxyl groups, besides removing undesirable non-magnetic species from the surface, by 0.5 M HCl (Belyavskii et al. 2006). The particles were carefully washed afterwards in distilled water, ethanol and acetone. A decantation process was carried out with a help of an external magnet; this occurring two times with each of the abovementioned liquids, and the mixture was mixed for approximately 10 min, followed by further drying at 60 °C under the pressure of 200 mbar. These treated particles were designated as CIP-0.

In the next step, the CIP-0 was modified with APTES to introduce $–NH_2$ groups onto their surface (Belyavskii et al. 2006; Cvek et al. 2015b) that could serve to facilitate the growth of PAMAM dendrons. The CIP-0 particles (~44 g) were treated in a mixture of a redundant amount of toluene (200 ml) and APTES (5 ml) at 110 °C under vigorous stirring and in a reflux system. After such treatment, the particles were rinsed and dried as previously. These particles were designated as CIP-APTES.

The dendrons were grown in accordance with a synthesis procedure reported in the literature (Fréchet and Tomalia 2001). The dried CIP-APTES particles were mixed with anhydrous methanol and MA was added drop-wise, where the amount of MA was in proportion to the molar ratio 2:1 to the amount of APTES. The reaction took place in an N_2 atmosphere, under vigorous stirring (250 rpm) and the fixed temperature of 5 °C for the first hour. Subsequently, the reaction proceeded for 24 h at room temperature. The particles were washed after treatment and dried as described previously. Following this, they were mixed with the anhydrous methanol and ED was subsequently added drop-wise; the amount of ED was in proportion to the molar ratio 1:1 to MA, as previously described. The reaction was performed under an N_2 atmosphere and vigorous stirring (250 rpm), and maintained at 5 °C for the first hour. The reaction ran for 30 h at room temperature, upon which the particles were rinsed again and dried following the procedure given above.

The reaction of the particles with MA and ED was repeated several times, until particles of generation GX had been prepared, where X represents the number of reactions with both MA and ED (see Fig. 1). Finally, the CIPs with PAMAM dendrons of G2 and G2.5 were obtained, the particles of which being designated as CIP-PAMAM-G2 and CIP-PAMAM-G2.5, respectively.

Particle characterization

Sample imaging took place on a high-resolution transmission electron microscope (HR-TEM) JEM 2100 (JEOL Japan), operated at the acceleration voltage of 180 kV, and equipped with a LaB6 cathode and a 5 megapixel TENGRA camera

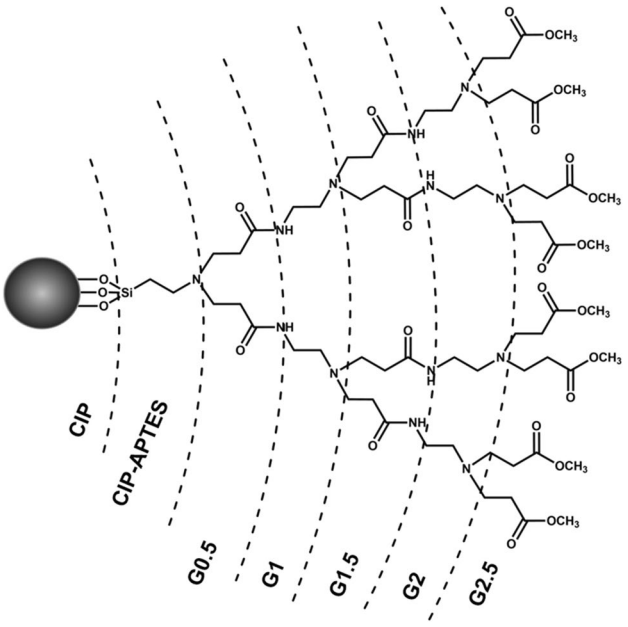

Fig. 1 Schematic illustration of the hypothetical chemical composition and structure of the PAMAM dendron on the CIP

(Olympus, Germany). The diluted sample suspensions in methanol (5 mg/ml) were drop-cast onto carbon-coated copper grids with a mesh size of 300 (Structure Probe Inc., USA) and dried at 70 °C. The prepared particles were further characterized by diffuse reflectance infrared Fourier transform spectroscopy (DRIFT; Nicolet 6700, Thermo Scientific, USA) in combination with KBr, Dispersive Raman microscopy (Nicolet DXR, Thermo Scientific, USA) and energy dispersive X-ray spectroscopy (EDX) performed on an Octane SSD (area of 30 mm^2) EDX detector (AMETEC) integrated into a scanning electron microscope (Nova NanoSEM 450, FEI company, Japan). Magnetic curves for the prepared samples were measured on a vibration sample magnetometer (VSM; Model 7404, Lake Shore, USA) in the magnetic field range of ± 760 kA m^{-1} at room temperature. Thermogravimetric analysis (TGA) was performed on a thermogravimetric analyser (TGA Q500, TA Instruments, USA) at a temperature range of 25–800 °C in an N_2 atmosphere at a heating rate of 10 °C min^{-1}. X-ray photoelectron spectroscopy measurements were gauged on a TFA XPS device (Physical Electronics). The base pressure in the XPS analysis chamber equalled approximately 6×10^{-8} Pa. The samples were excited by X-rays over a 400-μm^2 spot area with monochromatic Al $K\alpha_{1,2}$ radiation at 1486.6 eV. Photoelectrons were detected by a hemispherical analyser positioned at an angle of 45° from normal with respect to the sample surface. Survey scan spectra were acquired at a pass energy of 187.85 eV and an energy step of 0.4 eV, whereas for Fe 2p, C 1 s, O 1 s, N 1 s and Si 2p, individual high-resolution spectra were taken at the pass energy of 29.35 eV and energy step of 0.125 eV. All the spectra were referenced to the main C 1 s

peak of the carbon atoms, which had been assigned a value of 284.8 eV. The spectra were analysed in MultiPak v8.1c software (Ulvac-Phi, Japan) from Physical Electronics, which came supplied with the spectrometer.

Preparation of magnetorheological suspensions and their characterization

Magnetorheological suspensions containing 60 wt% of the particles were prepared by dispersing the particles within the silicone oil. Thus, three different MR formulations containing CIP-0, CIP-PAMAM-G2 and CIP-PAMAM-G2.5 particles were fabricated and labelled as MRS-0, MRS-PAMAM-G2 and MRS-PAMAM-G2.5. Prior to each measurement, the suspensions were thoroughly homogenized by mechanical mixing and ultrasonication (K-12LE, Kraintek, Slovakia).

Magnetorheological measurements were performed on a rotational rheometer (MCR 502 Anton Paar, Austria), with an external magnetic cell and gapped parallel plates of 300 µm (the width between the upper and lower) in the presence of an external magnetic field of intensity 0–438 kA/m at 25 °C. MR characterization was conducted in shear test mode, involving both controlled shear rate (CSR) and controlled shear stress (CSS). Measurement for the former was performed at the shear rate of 0–80 s^{-1}; in the case of the latter, firstly measurements at the constant shear rate of 50 s^{-1} were taken to obtain a value for shear stress, τ_{50}, and subsequently a CSS ramp from 0 Pa to τ_{50} was applied.

Sedimentation stability was evaluated on a Krüss K100 Tensiometer (MK2/SF/C, Germany) fitted with a SH0640 measuring probe, in the shape of an upside-down umbrella. The measuring technique adopted was recently introduced, based on weight gain by the particles, which settled into the probe immersed in the tested suspension after a certain period of time (Sedlacik and Pavlinek 2014). Diluted MR suspensions containing 10 wt% of the particles were used for this purpose.

Diluted MR suspensions supplemented with 20 wt% of the particles in silicone oil were investigated by optical microscopy analysis. The samples were homogenized, then put between two glass slides, and a magnetic field with magnetic flux density of 120 mT was applied to create chain-like structures. The suspensions were observed on an optical microscope (Leica DVM2500, Germany) linked to a digital camera.

Results and discussion

XPS analysis revealed that the CIP particles had been successfully coated with APTES, in addition to further growth of the PAMAM dendrons (Li et al. 2016; Yin et al. 2015). While the bare CIP particles only showed the presence of carbon, oxygen and iron, the CIP-APTES particles possessed nitrogen and silicon from the APTES (Table 1). The carbon spectrum for sample CIP-APTES was similar to that for the bare CIP sample (Fig. 2a). In both cases, C–C, C–OH and C = O groups were observed; however, the oxygen spectrum differed for the sample with APTES (Fig. 2b); two peaks were clearly visible—besides oxygen from the oxidized iron, oxygen from the organic coating was evident. The CIP-APTES sample showed a clear N 1 s peak (Fig. 3). The nitrogen peaks for CIP-PAMAM-G2 and CIP-PAMAM-G2.5 approximated the one for APTES (Fig. 3). Since nitrogen is known for very slight chemical shifts in binding energy, it is not possible to distinguish different configurations of nitrogen in functional groups such as amino, amide or  , the presence of which would be expected according to Fig. 1.

Unlike nitrogen, the carbon spectra for CIP-PAMAM-G2 and CIP-PAMAM-G2.5 revealed significant differences from the carbon spectra for the CIP-APTES and CIP samples. The carbon spectra for the samples CIP-PAMAM-G2 and CIP-PAMAM-G2.5 were much wider than for CIP-APTES and CIP, indicating the presence of different functional groups originating from the PAMAM (Fig. 4). Fitting the carbon spectra for the samples, CIP-PAMAM-G2 and CIP-PAMAM-G2.5 showed some similarities, as functional groups such as C–OH/C–NH_2, C = O/N–C = O and O = C–OR were observed in both. Nevertheless, while the concentration of C–OH/C–NH_2 and C = O/N–C = O was almost the same, the concentration of O = C–OR was much higher for the sample CIP-PAMAM-G2.5 since acrylate constituted its top layer.

Figure 5 shows TEM images of a bare particle and its modified analogues, demonstrating that the samples CIP-PAMAM-G2 and CIP-PAMAM-G2.5 clearly possessed a layer of coating on the surface of the particles. While CIP-0 had bare particles, a sharp contrast between the iron particle and background could be discerned. In the case of particles CIP-PAMAM-G2 and CIP-PAMAM-G2.5, a thin layer was distinguishable, confirming the formation of PAMAM dendrons on the surface of the CIP. The thickness (< 30 nm) observed is highly desirable in the context of magnetorheology, since suppression of chemical and thermal oxidation

Table 1 Surface composition of the prepared samples in atomic per cent; the data were obtained from XPS analysis

Sample	C	O	Fe	N	Si
CIP	31.9	52.7	15.4		
CIP-APTES	46.3	31.0	3.4	6.6	12.8
CIP-PAMAM-G2	49.2	30.8	3.0	10.5	6.4
CIP-PAMAM-G2.5	49.7	31.0	3.0	8.8	7.5

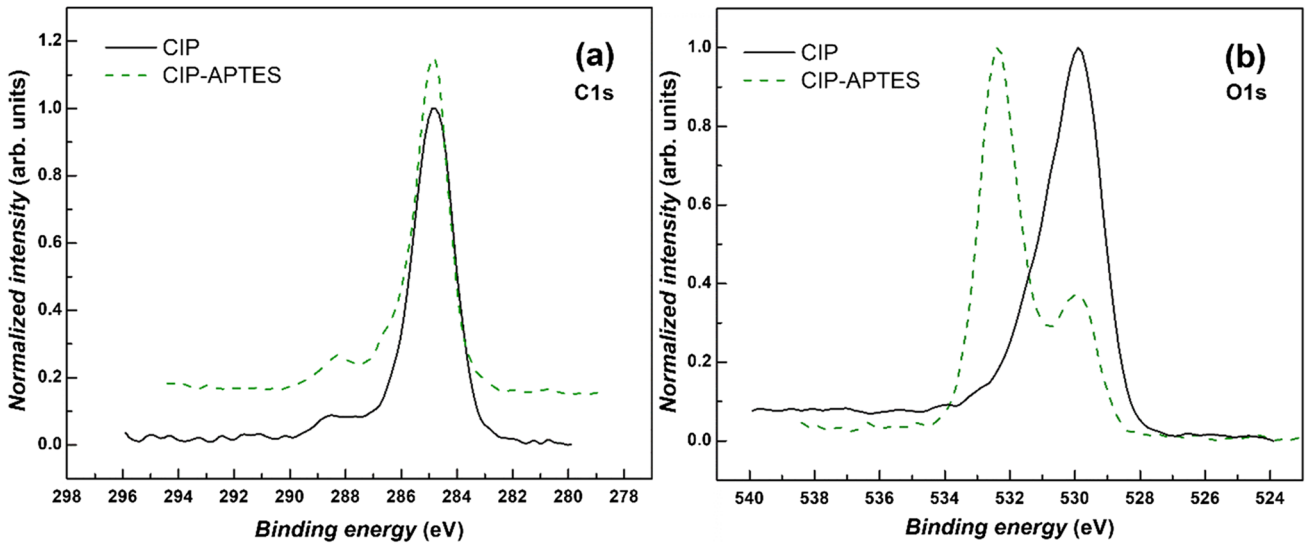

Fig. 2 Comparison of XPS high-resolution spectra for **a** C1s and **b** O1s of the CIP and CIP-APTES particles

of the particles is presumed to occur when values for M_s are maintained (Cvek et al. 2015a, b). It is worthy of note that the theoretical thickness of the layers, according to Fig. 1, was significantly less than the thickness detected. It is known that during silanization of a surface with APTES, obtaining a monolayer of APTES is difficult to achieve. It is more likely that, under certain reaction conditions, a silane layer of ca 10 nm thick on the surface is possible (Aissaoui et al. 2012). A recognized aspect is that growth of a generation 2 PAMAM dendrimer can bring about rise in particle size by about 8 nm (Khodadust et al. 2013). In the case of dendron growth, some side reactions may occur due to the given concentrations of the monomers and reaction conditions; furthermore, due to polarization forces and adsorption, a dendrimer has the potential to increase the size of the particles to 15 nm (Baykal et al. 2012; Jafari-Soghieh et al. 2019). The thicker layer discerned in this study could have been caused by either a trace amount of precursors remaining on the particles after the washing cycle or the chosen precursor ratio.

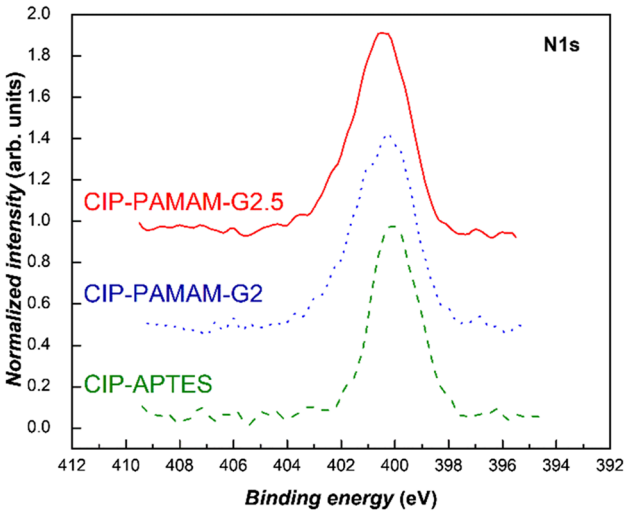

Fig. 3 XPS high-resolution spectra of N1s for the samples CIP-APTES, CIP-PAMAM-G2 and CIP-PAMAM-G2.5

The DRIFT spectra for the prepared samples showed a broad band in the region above 3200 cm^{-1} and a medium band at 1628 cm^{-1}, ascribed to the moisture of the samples (Fig. 6a). The sample CIP-PAMAM-G2.5 also exhibited peaks at 2921 cm^{-1} and 2856 cm^{-1} typical for PAMAM dendrons or dendrimers (Gautam et al. 2015; Parsian et al. 2016), representing the stretching of the functional groups $–CH_3$ and $–CH_2$, respectively. However, no other significant peaks were presented due to very thin layer of PAMAM dendrons on the surface of the CIPs (Fig. 5).

Figure 6b details the Raman spectra for the bare CIP and PAMAM samples. These spectra are not influenced by moisture, which significantly deteriorates infrared measurements and associated bands that prevail in FTIR findings. Raman analysis clearly confirmed that the PAMAM dendrons were present in both CIP-PAMAM samples. CIP-PAMAM-G2.5 contained acrylate groups corresponding to bands at 1745 cm^{-1} and 1320 cm^{-1}, representing C = O and C–O–C stretching, respectively; weak bands were also visible at 1040 cm^{-1} and 820 cm^{-1} pertaining to skeletal vibrations of MA. The spectrum for CIP-PAMAM-G2 included bands at 1732 cm^{-1} and 1035 cm^{-1}, which probably constituted C = O stretching from the O = C–NH–C– group and C–N stretching, respectively. The two spectra outlined above comprised similar bands; however, interpretation of them was informed by the fact that G2 and G2.5 contained acrylate

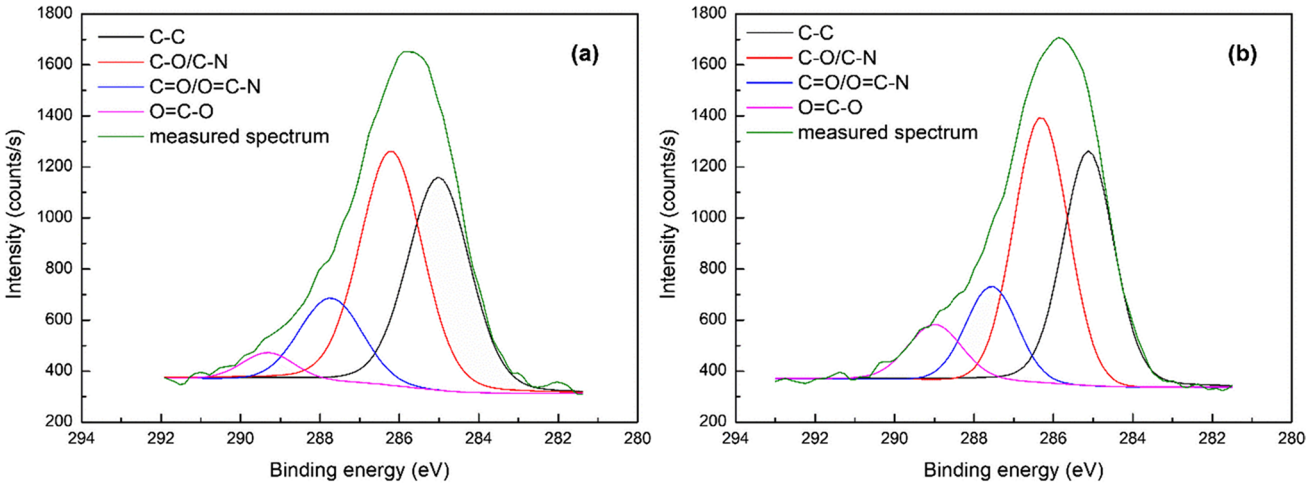

Fig. 4 Carbon C1s spectra with subcomponents for the samples **a** CIP-PAMAM-G2 and **b** CIP-PAMAM-G2.5

and amine (amide) groups, respectively. The spectra for both CIP-PAMAM samples featured bands in the regions 3000–2800 cm^{-1} and 1460–1455 cm^{-1}, confirming the presence of CH groups. Interestingly, the spectrum for Fe is typical for Fe_2O_3, due to possible oxidation of the surface layer of the particles, with no indication of acrylate and amine groups. This confirmed that binding MA and ED to CIP-0 in stepwise synthesis had been successful and CIP-PAMAM particles had been created. It was not possible to carry out precise differentiation of the G2 and G2.5 dendrons any further with vibrational spectra, as certain Raman bands (e.g. C = O, N–C, N–H and others) were present in the Raman spectra and, thus, also in both CIP-PAMAM samples. This result corresponded to EDX analysis.

Table 2 lists the results of EDX, a semi-quantitative analysis describing the chemical composition of a surface of a material (from depth upwards, in units of µm). Besides iron, the CIP-0 sample contained a small amount of carbon and oxygen, the former originating from iron pentacarbonyl—a precursor for preparing CIPs, while the latter comes from the hydroxyl groups on the surface of the particles; however, it is not possible to fully disprove the presence of iron oxide. As for CIP-PAMAM-G2 and CIP-PAMAM-G2.5, the small portions of nitrogen and silicon from the APTES and PAMAM dendrons confirmed that the coating process of the CIP-0 with PAMAM dendrons had taken place successfully.

The value for M_S of the magnetic particles is important in relation to the MR effect of an MRS. In low magnetic fields, yield stress (τ_y)—the minimal amount of stress that has to be applied before the system starts to flow—is primarily dependent on magnetic field intensity, scaling as $\tau_y \sim H^2$; with increase in the intensity of the magnetic field, M_S emerges as an important parameter, and τ_y scales as $\tau_y \sim M_S^{1/2} H^{3/2}$ (Fang et al. 2011; Ginder et al. 1996). It is consequently crucial to follow a controlled procedure for coating magnetic particles in order to keep values for M_S as high as possible. Herein,

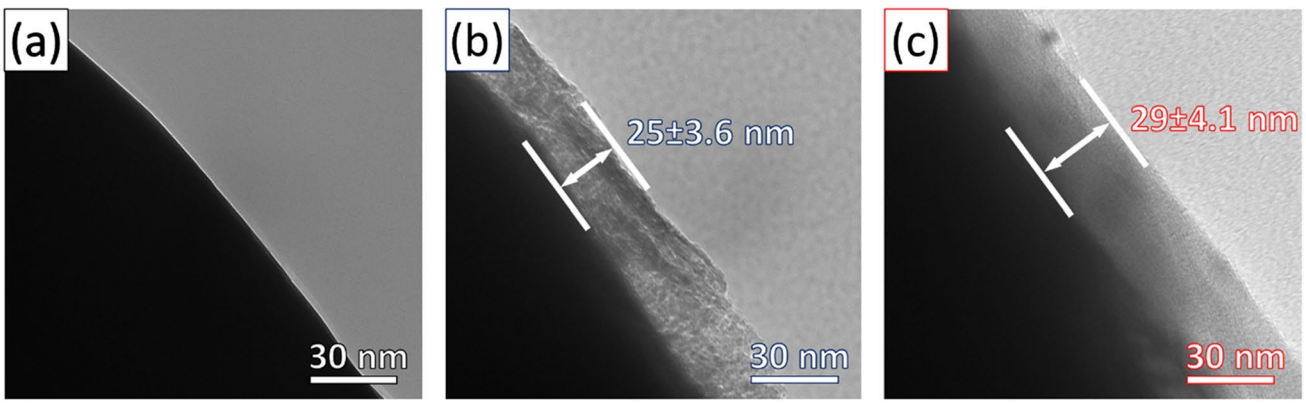

Fig. 5 TEM images of **a** the bare CIP-0 and its analogues, **b** CIP-PAMAM-G2 and **c** CIP-PAMAM-G2.5

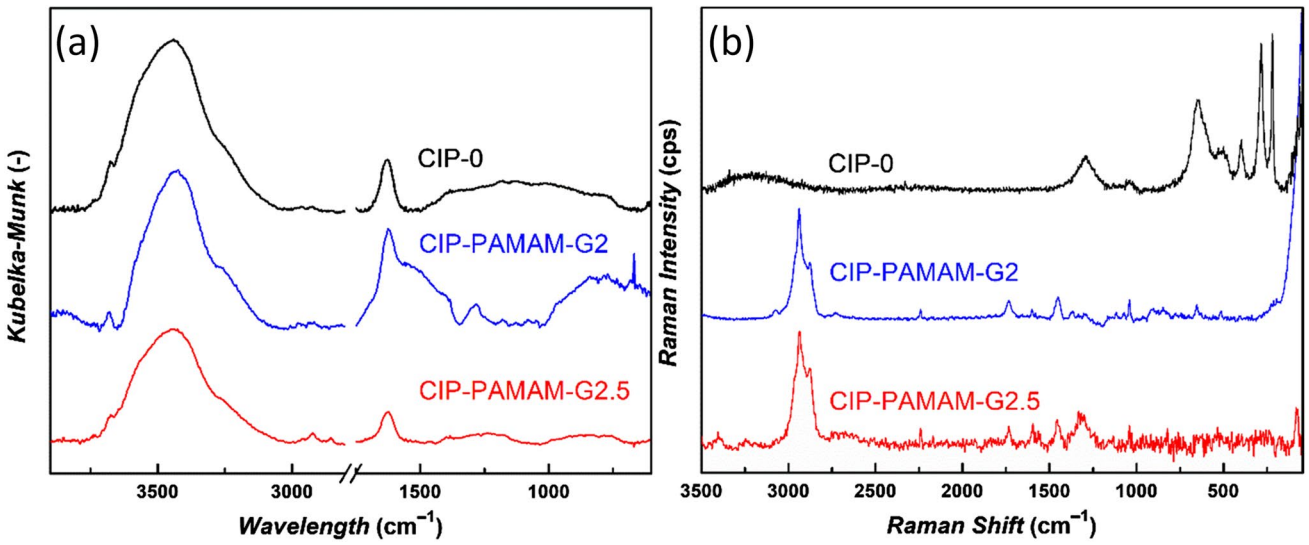

Fig. 6 DRIFT (**a**) and Raman (**b**) spectra for the bare CIP-0 and its analogues CIP-PAMAM-G2 and CIP-PAMAM-G2.5

the CIP coating process only subtly affected the M_S values for the prepared particles (Fig. 7), which is a desirable quality for an MRS since its MR effect persists correspondingly. The M_S values for the samples are given in Table 2, revealing that the M_S for the sample with the greatest dendron generation of a non-magnetic layer on its surface (CIP-PAMAM-G2.5) merely decreased by about 4.7% compared to the neat CIPs (CIP-0). This finding is similar to the lowest drop in M_S values found in the literature, wherein atom transfer radical polymerization was employed for controlled application of layers of a polymeric coating on CIPs (Cvek et al. 2015b).

Table 2 Results of EDX analysis (values are given in weight percent) and the saturation magnetization values for the prepared particles

Element	CIP-0 (wt%)	CIP-PAMAM-G2 (wt%)	CIP-PAMAM-G2.5 (wt%)
C	3.06 ± 0.18	2.88 ± 0.19	3.37 ± 0.20
N	–	0.38 ± 0.17	0.43 ± 0.19
O	1.28 ± 0.09	1.14 ± 0.10	1.13 ± 0.11
Si	–	0.15 ± 0.03	0.13 ± 0.03
Fe	95.66 ± 0.20	95.18 ± 0.26	94.94 ± 0.29
Magnetic saturation M_S (emu/g)	207.0	197.7	197.3
Decrease in M_S against CIP-0 (%)	-	4.5	4.7

Oxidation stability in an acidic solution is a test often performed to gauge improvement in chemical stability and confirm the presence of a compact coating on particles. Rise in pH value during the treatment of CIP-0 in 0.05 M solution of HCl (Fig. 8a) indicated that oxidation of the particles had occurred, evident through neutralization of the acidic solution. In contrast, CI-PAMAM-G2 and CI-PAMAM-G2.5, with a thin layer of coating on their respective surfaces, showed high stability in acidic conditions, confirming the PAMAM coating was free of defects and able to inhibit contact between the acidic solution and the iron core. This extreme stability suggests that the uniform coating in place could additionally protect the iron particles from entry by moisture or other substances containing oxygen during use,

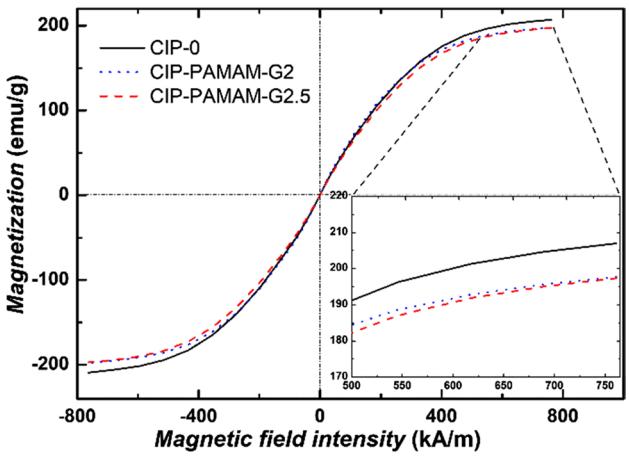

Fig.7 Magnetic curves for the bare CIP-0 and its analogues CIP-PAMAM-G2 and CIP-PAMAM-G2.5

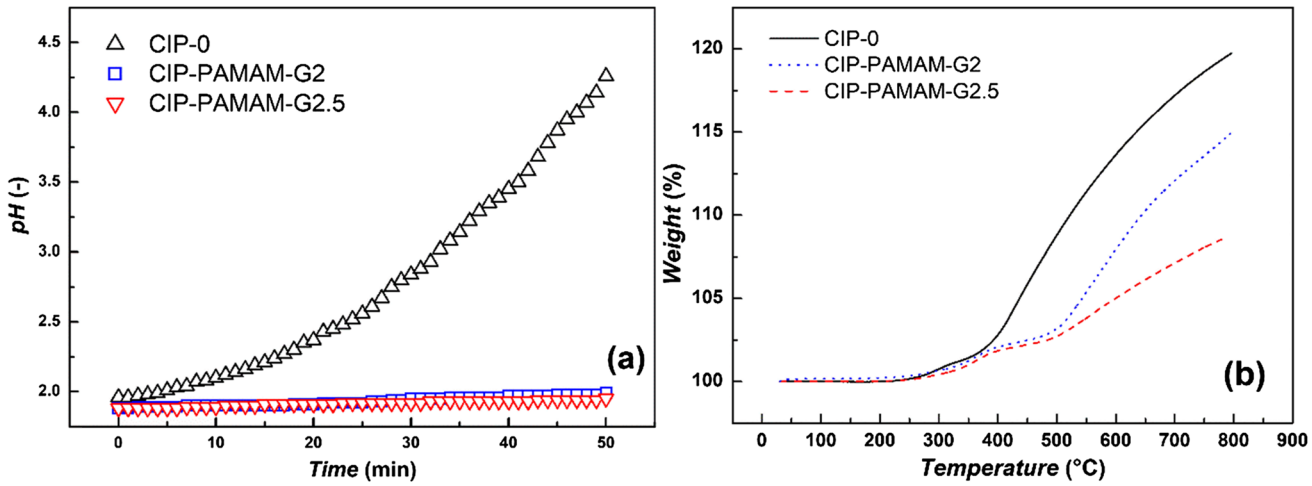

Fig 8 **a** Oxidation stability of the bare CIP-0 and its analogues CIP-PAMAM-G2 and CIP-PAMAM-G2.5, as tested in 0.05 M solution of HCl at room temperature in relation to the dependence of pH values of the solution over time. **b** TGA curves for the bare CIP-0 and its analogues CIP-PAMAM-G2 and CIP-PAMAM-G2.5, as tested in an N_2 atmosphere at a heating rate of 10 °C min^{-1}

thus preventing oxidation from affecting the service life of any instruments featuring them. Figure 8b depicts the change in weight exhibited by the prepared particles during heat treatment in a N_2 atmosphere at up to 800 °C. In the case of CIP-0, the particles were stable until 370 °C, whereupon an abrupt gain in weight by the particles occurred. Even though the test happened in a N_2 atmosphere, the weight of the samples increased considerably during the heating process. The gain in weight could rise from initiation of a nitriding phase, causing formation of Fe_4N or various Fe_3N_x (Konig et al. 2017). Nevertheless, the particles still possessed omnipresent oxygen adsorbed to their surfaces with the potential to oxidise them. The coated particles demonstrated improved thermal stability upon a sudden increase in weight at 500 °C. It has been stated in the literature that—concurrent with or following thermal decomposition of a polymeric layer—should a nitriding phase develop or the particles oxidise, thermal decomposition of the polymer still takes place, despite the fact that no decrease in weight is evident (Cvek et al. 2015b).

Magnetorheology and sedimentation stability

The MRSs exhibited transition from liquid to a solid-like state after applying an external magnetic field, a typical characteristic for an MRS. In the absence of an external magnetic field, they demonstrated slightly pseudoplastic behaviour, whereas in a presence of one, their values for shear stress increased by several orders of magnitude and they exhibited field-dependent values for τ_y (Fig. 9) (Anupama et al. 2019; Kwon et al. 2020). Several rheological models are capable of estimating τ_y for an MRS. Even though some exist with the capability to fit flow curves (Cvek et al. 2016, Seo, Han, Choi, Takahara, Choi and Seo 2018), for reasons of feasibility and simplicity, herein the classic Herschel-Bulkley (H-B) rheological model was employed to fit the experimental data. The H-B equation is expressed below (Eq. 1), where K represents the consistency index and n is the non-Newtonian flow index.

$$\tau = K \bullet \dot{\gamma}^n + \tau_y \tag{1}$$

The field-off viscosities of the MRSs based on coated particles have the potential to slightly exceed the value for MRS-CIP, since the branched polymeric surfaces on CI-PAMAM-G2 and CI-PAMAM-G2.5 increase interactions between both them and the carrier fluid (silicone oil), which brings about a minor decrease in the parameter n from 0.89 to 0.84 that describes the evolved pseudoplasticity of the system (Table 3). Interestingly, values for τ_y are higher for the MRSs based on coated particles than MRS-CIP (Table 3). The polymeric coating should hinder possible particle agglomeration and improve the arrangement of particles upon application of a magnetic field, thereby enhancing the MR effect of the MRS (Lopez-Lopez et al. 2008b). When tested with the strongest applied magnetic field of 438 kA m^{-1}, the MRSs with coated particles (CI-PAMAM-G2 and CI-PAMAM-G2.5) exhibited τ_y values approximately 4.8% and 4.0% higher than the reference MRS, respectively. Thus, the ability to control the thickness of the organic layer on magnetic particles in an MRS could result in suitable particles with significantly heightened oxidation stability as well as the absence of any undesirable decrease in MR performance by the MRS.

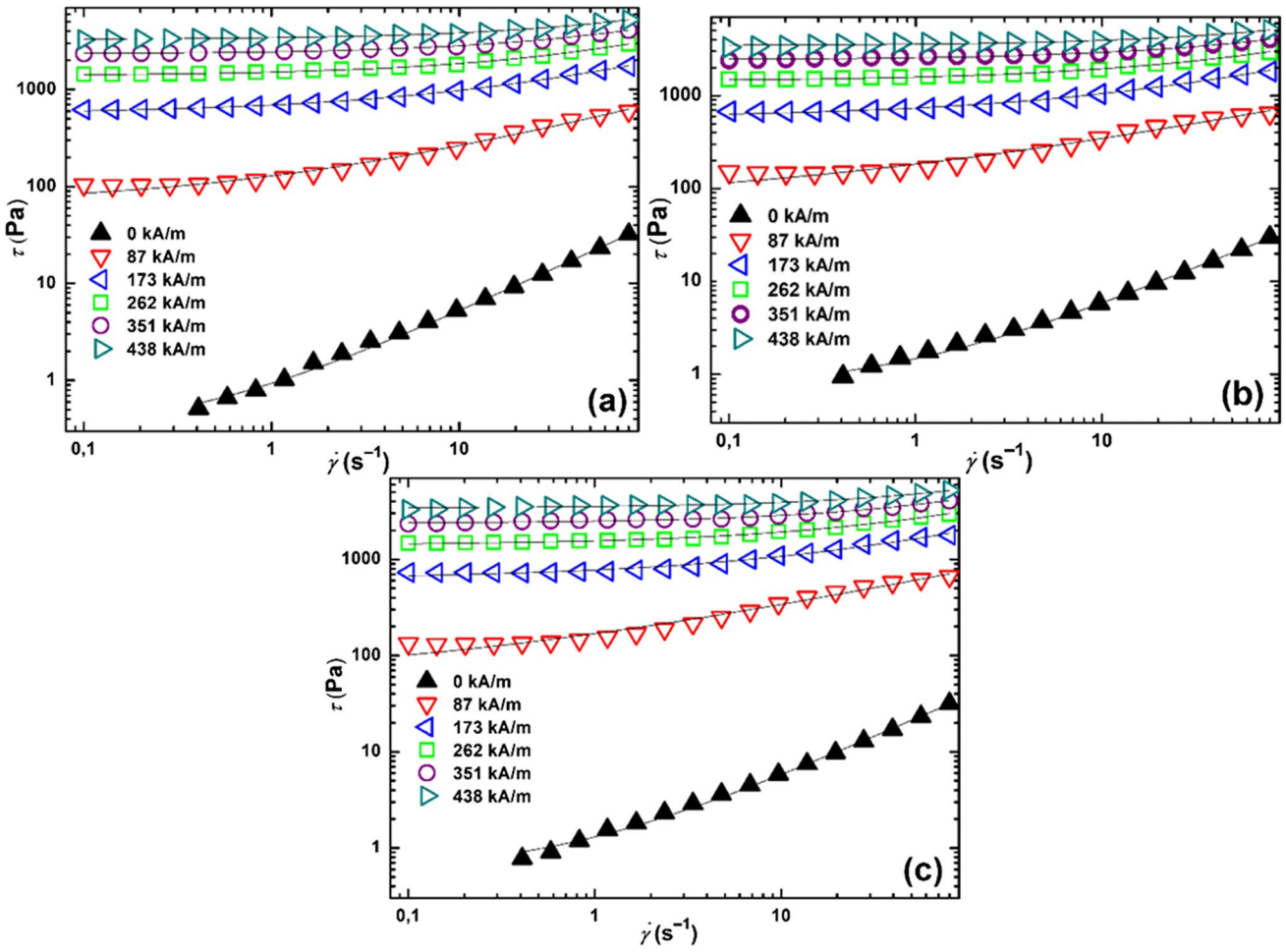

Fig. 9 Log–log dependencies of shear stress on the shear rate for the prepared MRSs: **a** MRS-CIP, **b** MRS-PAMAM-G2 and **c** MRS-PAMAM-G2.5 in various magnetic fields; measurements were performed in CSR mode, and the solid lines represent the H-B fit

Table 3 Values for rheological parameters obtained from the H-B model and τ_{stat} values for the prepared MRSs at various intensities of magnetic field

Sample	Parameter	Magnetic field intensity (kA/m)					
		0	87	173	262	351	438
MRS-CIP	n [-]	0.89	0.50	0.51	0.58	0.60	0.61
	K [Pa s^n]	0.64	63	128	121	127	137
	τ_y [Pa]	0.29	65	563	1 390	2 320	3 290
MRS-PAMAM-G2	n [-]	0.85	0.31	0.45	0.54	0.59	0.64
	K [Pa s^n]	0.76	113	147	147	130	124
	τ_y [Pa]	0.71	70	597	1 440	2 430	3 450
MRS-PAMAM-G2.5	n [-]	0.85	0.40	0.49	0.55	0.60	0.64
	K [Pa s^n]	0.73	112	144	144	124	110
	τ_y [Pa]	0.57	57	629	1 410	2 370	3 420
Static yield stress values	Parameter	Magnetic field intensity (kA/m)					
		0*	87	173	262	351	438
MRS-CIP	τ_{stat} [Pa]	–	239	961	1870	2920	4140
MRS-PAMAM-G2	τ_{stat} [Pa]	–	261	817	1880	2960	4000
MRS-PAMAM-G2.5	τ_{stat} [Pa]	–	219	910	1760	2850	3930

*The prepared MRSs did not exhibit any inherent τ_{stat}

Another way to evaluate the stiffness of an MRS is to determine static yield stress, denoted as τ_{stat}, and different methods exist to do so experimentally (De Vicente et al. 2010; Yang et al. 2009). Controlled shear stress measurement, with an ascending shear stress ramp rising to the value τ_{50}, was employed for this purpose. In this context, no macroscopic flow occurs in the system below τ_{stat}, as represented by high values for viscosity. When the value for shear stress exceeds that for τ_{stat}, flow is initiated and an abrupt drop in viscosity is observed (Fig. 10). The final value recorded for shear stress before such dramatic reduction in viscosity is designated as τ_{stat} (De Vicente et al. 2010; Fang et al. 2011). In tests, unlike the τ_y values, τ_{stat} was found to be higher for MRS-CIP than systems with coated particles, even though the difference is less than < 6% at the magnetic field intensity of 438 kA m^{-1} (Table 3). It should be further noted that τ_{stat} values were generally higher than τ_0 values due to the different origins of both phenomena and methods for their estimation. While τ_y is estimated by indirect methods (De Vicente et al. 2011), τ_{stat}, which is often referred to as frictional yield stress, is considered collapse of the top layer of a built-up structure close to the moving part of its geometry (or "slip"), rather than the collapse of built-up structures throughout the MRS (Volkova et al. 2000). Having a coating on the particles can prevent them from agglomerating and facilitate enhanced arrangement of them upon application of a magnetic field as a consequence; in addition, they demonstrate higher τ_y values than bare CIPs (Lopez-Lopez et al. 2008b). In the case of τ_{stat}, its values are not significantly affected by such built-up structures, since particles collapse from the top part of the measured geometry.

The fact that CIP formed agglomerates in the silicone oil is evident from images obtained from optical microscopy (Fig. 11a). Since such particles possess a polar surface, they tend to group together in silicone oil. The coated surfaces of those in CIP-PAMAM-G2 and CIP-PAMAM-G2.5 led to good dispersion in the liquid medium, both exhibiting a low amount of agglomerates of small size compared to CIPs (Fig. 11c, e). After applying a magnetic field, the particles created chain-like structures in the direction of the magnetic field (Fig. 11b, d, f). While thick CIP chains of agglomerates were evident, CIP-PAMAM-G2 and CIP-PAMAM-G2.5 created

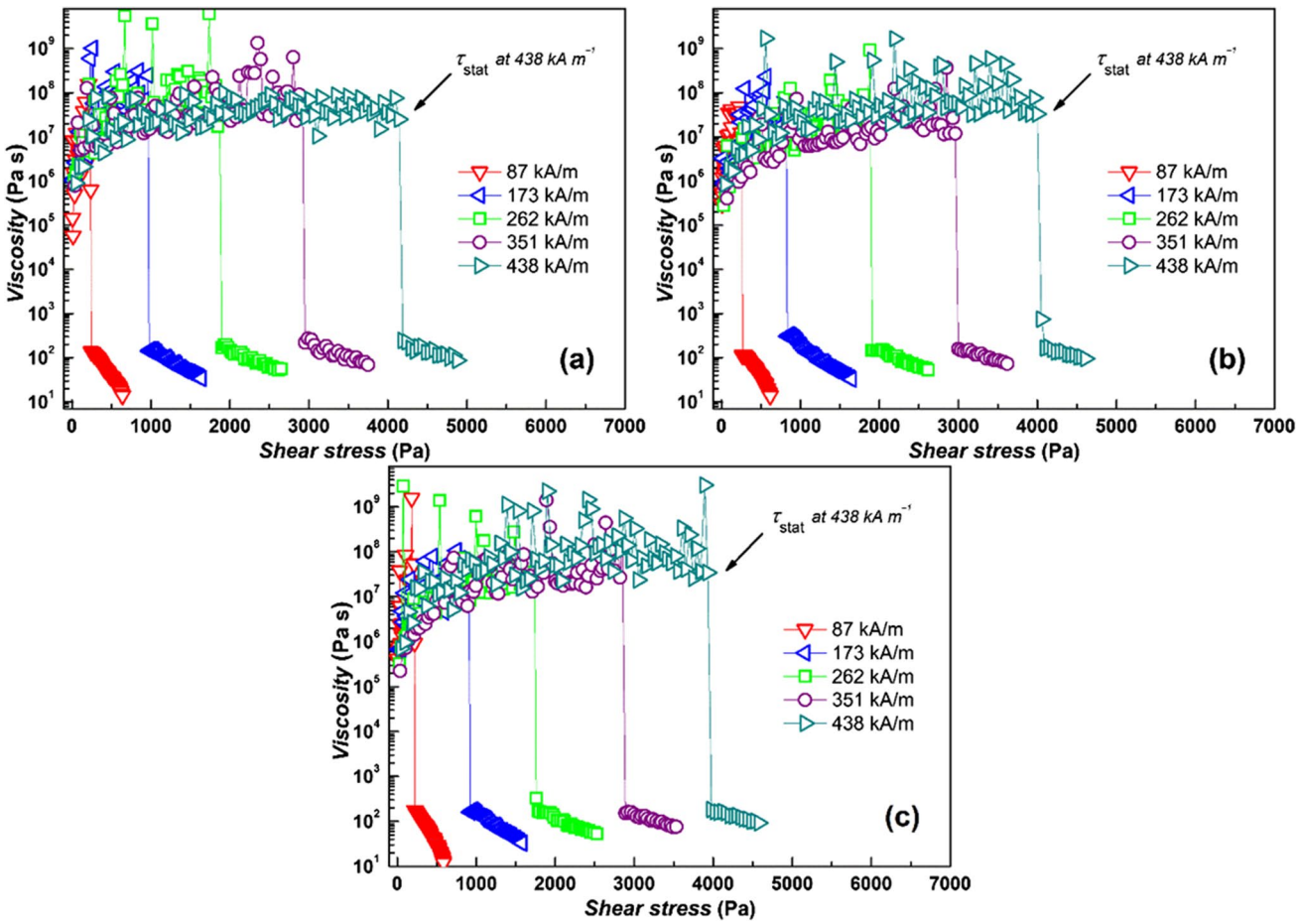

Fig. 10 Dependencies of viscosity on shear stress for the prepared MRSs: **a** MRS-CIP, **b** MRS-PAMAM-G2 and **c** MRS-PAMAM-G2.5 in various magnetic fields; measurements were performed in CSS mode

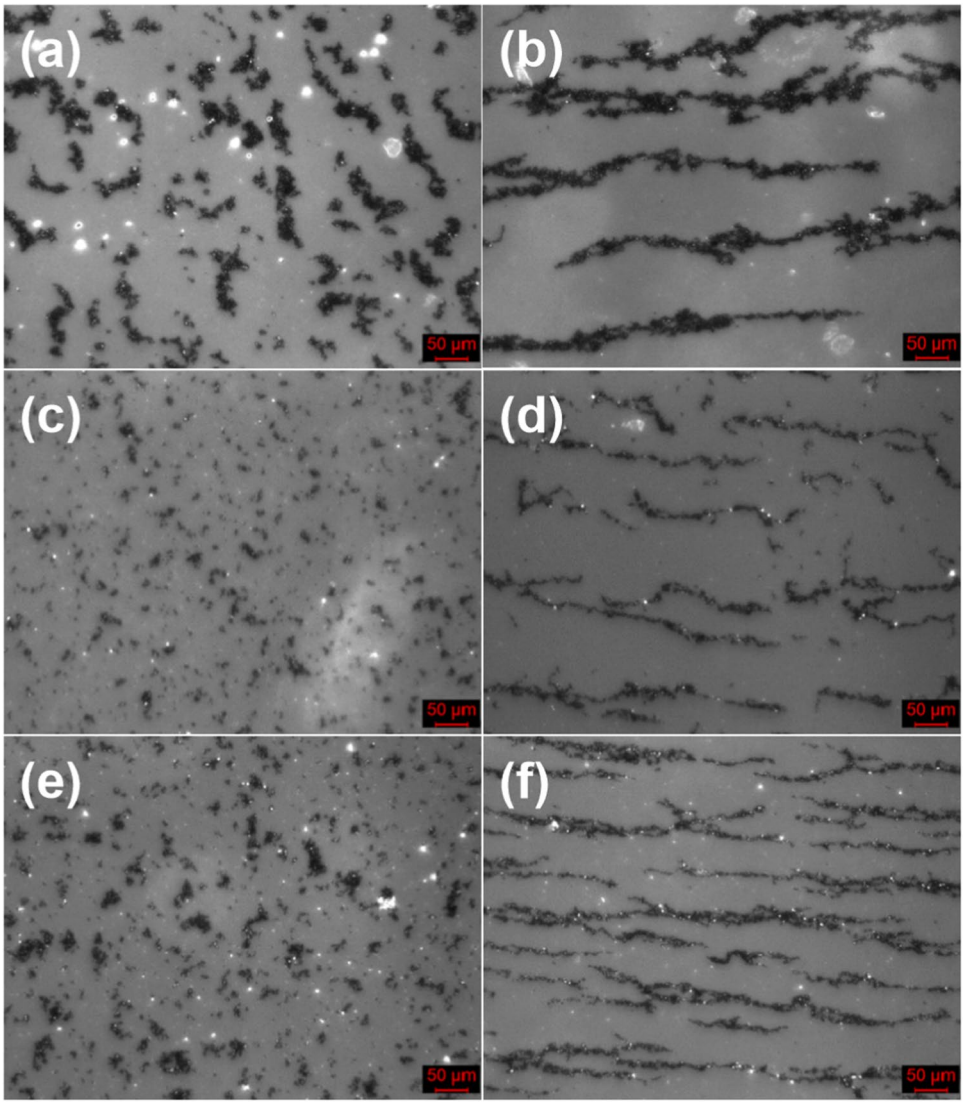

Fig. 11 Optical microscopy of 20 wt% silicone oil suspensions of **a**, **b** CIP-0, **c**, **d** CI-PAMAM-G2 and **e**, **f** CI-PAMAM-G2.5. Images **a**, **c** and **e** are taken in the absence of a magnetic field; images **b**, **d** and **f** are taken in the presence of a magnetic field with magnetic flux density of 120 mT

thinner columns of coated particles that were more uniform than the CIP chains. Comparing CIP-PAMAM-G2 and CIP-PAMAM-G2.5 with a terminating $–NH_2$ group or $–O–CH_3$, the former demonstrated less aggregation than the latter.

Poor sedimentation stability is another drawback of MRSs that has to be overcome for possible everyday applications. Although the coating process of the particles itself does not provide MRSs with long-term stability, it can reduce the sedimentation rate of the particles, which takes place through decrease in overall density of the particles and heightened friction forces between the particles and carrier fluid. Furthermore, coating the particles also diminishes their tendency to agglomerate, potentially lending the system greater stability (Lopez-Lopez et al. 2008a). Figure 12 details measurements of sedimentation stability for the prepared MRSs. These describe a comparative approach for the given MRSs and are expressed as t_{90}, i.e. the time in which 90% of the particles from the

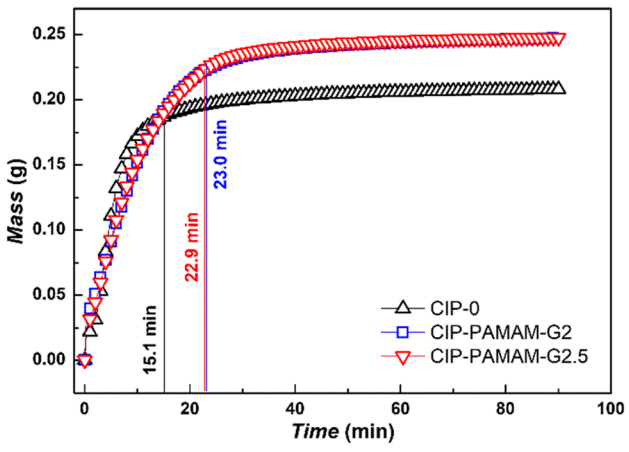

Fig. 12 Test of sedimentation stability of the prepared MRSs; results are expressed as the mass of particles settled in the measuring probe over a certain period of time

area above the probe settle into it. While t_{90} was 15.1 min for MRS-CIP, the same for the two MRSs based on the PAMAM-coated particles were found to be ~ 23.0 min. for both. Unfortunately, it is not possible to compare the findings with another MRS due to unique nature of the sedimentation testing method adopted.

Conclusions

This paper presents application of a coating of carbonyl iron particles with poly(amidoamine) dendrons as an efficient means for preventing particle oxidation and extending the service life of suspensions. The particles were coated with poly(amidoamine) of 2 and 2.5 generations, giving rise to different functional groups on their surfaces. The thickness of the dendritic layers equalled approximately 30 nm, which provided sufficient thermal and chemical oxidation stability, as tested by thermogravimetric analysis and treatment in an acidic solution, thereby confirming the particles had been completely coated. In addition, their saturation magnetization decreased by only ca 4.5% compared to the bare carbonyl iron particles. The particles were further employed as a dispersed phase in magnetorheological suspensions, and their performance was investigated through measuring controlled shear rate and controlled shear stress in order to determine dynamic yield stress, conducted by means of the Herschel-Bulkley model and static yield stress. Interestingly, the magnetorheological suspensions based on coated particles exhibited values of ca 4% higher for dynamic yield stress, as well as demonstrating enhanced sedimentation stability, compared to magnetorheological suspensions based on the original carbonyl iron particles. Optical microscopy revealed that the organic layer on the surface hinders the coated particles from forming agglomerates; thus, as stated in the literature, the potential exists for developing MR suspensions with heightened magnetorheological effects. Such coated particles would appear to make it possible to prepare magnetorheological suspensions with high oxidation stability, thereby overcoming the issue of in-use-thickening which is known to limit the utilization of magnetorheological suspensions, with the consequent advantage of persistent high performance in the presence of a magnetic field. In addition, the improvement in reduced abrasion of the particles during their use can be expected.

Acknowledgements This work was supported by the Ministry of Education, Youth and Sports of the Czech Republic – DKRVO (RP/CPS/2020/003) and DKRVO (RP/CPS/2020/006). Research was also aided by the Operational Programme Research and Development for Innovations initiative co-funded by the European Regional Development Fund (ERDF) and the state budget of the Czech Republic, within the framework of a Centre of Polymer Systems project (CZ.1.05/2.1.00/19.0409).

Data availability The datasets generated and/or analysed during the current study are available from the corresponding author upon request.

Declarations

Conflict of interest The authors declare no competing interests.

References

Aissaoui N, Bergaoui L, Landoulsi J, Lambert JF, Boujday S (2012) Silane layers on silicon surfaces: mechanism of interaction, stability, and influence on protein adsorption. Langmuir 28:656–665. https://doi.org/10.1021/la2036778

Anupama AV, Kumaran V, Sahoo B (2019) Synthesis of highly magnetic Mn-Zn ferrite (Mn0.7Zn0.3Fe2O4) ceramic powder and its use in smart magnetorheological fluid. Rheol Acta 58:273–280. https://doi.org/10.1007/s00397-019-01137-z

Baykal A, Toprak MS, Durmus Z, Senel M, Sozeri H, Demir A (2012) Synthesis and characterization of dendrimer-encapsulated iron and iron-oxide nanoparticles. J Supercond Nov Magn 25:1541–1549. https://doi.org/10.1007/s10948-012-1454-z

Bell RC, Karli JO, Vavreck AN, Zimmerman DT, Ngatu GT, Wereley NM (2008) Magnetorheology of submicron diameter iron microwires dispersed in silicone oil. Smart Mater Struct 17:015028. https://doi.org/10.1088/0964-1726/17/01/015028

Belyavskii SG, Mingalyov PG, Giulieri F, Combarrieau R, Lisichkin GV (2006) Chemical modification of the surface of a carbonyl iron powder. Protect Met 42:244–252. https://doi.org/10.1134/s0033173206030064

Bombard AJF, Goncalves FR, de Vicente J (2015) Magnetorheology of carbonyl iron dispersions in 1-alkyl-3methylimidazolium ionic liquids. Ind Eng Chem Res 54:9956–9963. https://doi.org/10.1021/acs.iecr.5b02824

Bucchi F, Forte P, Franceschini A, Frendo F (2013) Analysis of differently sized prototypes of an MR clutch by performance indices. Smart Mater Struct 22:105009. https://doi.org/10.1088/0964-1726/22/10/105009

Carlson JD, Jolly MR (2000) MR fluid, foam and elastomer devices. Mechatronics 10:555–569. https://doi.org/10.1016/s0957-4158(99)00064-1

Chen ZQ, Wang XY, Ko JM, Ni YQ, Spencer BF, Yang G (2003) MR damping system on Dongting Lake cable-stayed bridge. In: Liu SC (ed) Smart structures and materials 2003: smart systems and nondestructive evaluation for civil infrastructures, vol 5057. Spie-Int Soc Optical Engineering, Bellingham, pp 229–235

Cvek M, Mrlik M, Ilcikova M, Mosnacek J, Babayan V, Kucekova Z, Humpolicek P, Pavlinek V (2015a) The chemical stability and cytotoxicity of carbonyl iron particles grafted with poly(glycidyl methacrylate) and the magnetorheological activity of their suspensions. RSC Adv 5:72816–72824. https://doi.org/10.1039/c5ra11968e

Cvek M, Mrlik M, Ilcikova M, Plachy T, Sedlacik M, Mosnacek J, Pavlinek V (2015b) A facile controllable coating of carbonyl iron particles with poly(glycidyl methacrylate): a tool for adjusting MR response and stability properties. J Mater Chem C 3:4646–4656. https://doi.org/10.1039/c5tc00319a

Cvek M, Mrlik M, Pavlinek V (2016) A rheological evaluation of steady shear magnetorheological flow behavior using three-parameter viscoplastic models. J Rheol 60:687. https://doi.org/10.1122/1.4954249

Cvek M, Torres-Mendieta R, Havelka O, Urbanek M, Plachy T, Cernik M (2020) Laser-induced fragmentation of carbonyl iron

as a clean method to enhance magnetorheological effect. J Clean Prod 254:120182. https://doi.org/10.1016/j.jclepro.2020.120182
de Vicente J, Vereda F, Segovia-Gutierrez JP, Morales MD, Hidalgo-Alvarez R (2010) Effect of particle shape in magnetorheology. J Rheol 54:1337–1362. https://doi.org/10.1122/1.3479045
de Vicente J, Klingenberg DJ, Hidalgo-Alvarez R (2011) Magnetorheological fluids: a review. Soft Matter 7:3701–3710. https://doi.org/10.1039/c0sm01221a
Demir M, Senel M, Baykal A (2014) Reversible immobilization of BSA on Cu-chelated PAMAM dendrimer modified iron oxide nanoparticles. Appl Surf Sci 314:697–703. https://doi.org/10.1016/j.apsusc.2014.07.082
Fang FF, Liu YD, Choi HJ, Seo Y (2011) Core-shell structured carbonyl iron microspheres prepared via dual-step functionality coatings and their magnetorheological response. ACS Appl Mater Interfaces 3:3487–3495. https://doi.org/10.1021/am200714p
Feijoo AV, Lopez-Lopez MT, Galindo-Gonzalez C, Stange S, Nguyen TT, Mammeri F, Merah S, Ponton A (2020) Rheological investigation of magnetic sensitive biopolymer composites: effect of the ligand grafting of magnetic nanoparticles. Rheol Acta 59:165–176. https://doi.org/10.1007/s00397-020-01191-y
Fréchet JMJ, Tomalia DA (2001) Dendrimers and other dendritic polymers. Wiley, Edithvale
Gautam SP, Keservani RK, Gautam T, Gupta AK, Sharma AK (2015) An alternative approach for acetylation of amine terminated polyamidoamine (PAMAM) dendrimer. Ars Pharmaceutica 56:155–159
Ginder JM, Davis LC, Elie LD (1996) Rheology of magnetorheological fluids: models and measurements. Int J Mod Phys B 10:3293–3303. https://doi.org/10.1142/s0217979296001744
Han S, Choi J, Seo YP, Park IJ, Choi HJ, Seo Y (2018) High-performance magnetorheological suspensions of pickering-emulsion-polymerized polystyrene/Fe_3O_4 particles with enhanced stability. Langmuir 34:2807–2814. https://doi.org/10.1021/acs.langmuir.7b04043
Han JK, Lee JY, Choi HJ (2019) Rheological effect of Zn-doped ferrite nanoparticle additive with enhanced magnetism on micro-spherical carbonyl iron based magnetorheological suspension. Colloid Surf A-Physicochem Eng Asp 571:168–173. https://doi.org/10.1016/j.colsurfa.2019.03.084
Jafari-Soghieh F, Maleki B, Behniafar H (2019) Effect of dendrimer-functionalized magnetic iron oxide nanoparticles on improving thermal and mechanical properties of DGEBA/IPD epoxy networks. High Perform Polym 31:24–31. https://doi.org/10.1177/0954008317749020
Khodadust R, Unsoy G, Yalcin S, Gunduz G, Gunduz U (2013) PAMAM dendrimer-coated iron oxide nanoparticles: synthesis and characterization of different generations. J Nanopart Res 15:1488. https://doi.org/10.1007/s11051-013-1488-6
Konig R, Muller S, Dinnebier RE, Hinrichsen B, Muller P, Ribbens A, Hwang J, Liebscher R, Etter M, Pistidda C (2017) The crystal structures of carbonyl iron powde - revised using in situ synchrotron XRPD. Z Krist-Cryst Mater 232:835–842. https://doi.org/10.1515/zkri-2017-2067
Kwon SH, Hong CH, Do PX, Choi SB, Choi HJ (2015) Magnetorheology of a carbonyliron microsphere suspension with a halloysite additive and its damping force characteristics. Ind Eng Chem Res 54:4655–4663. https://doi.org/10.1021/acs.iecr.5b00233
Kwon SH, Na SM, Flatau AB, Choi HJ (2020) Fe-Ga alloy based magnetorheological fluid and its viscoelastic characteristics. J Ind Eng Chem 82:433–438. https://doi.org/10.1016/j.jiec.2019.11.007
Lee JW, Hong KP, Kwon SH, Choi HJ, Cho MW (2017) Suspension rheology and magnetorheological finishing characteristics of biopolymer-coated carbonyliron particles. Ind Eng Chem Res 56:2416–2424. https://doi.org/10.1021/acs.iecr.6b03790
Li YZ, Guan YQ, Liu Y, Yin JB, Zhao XP (2016) Highly stable nanofluid based on polyhedral oligomeric silsesquioxane-decorated graphene oxide nanosheets and its enhanced electro-responsive behavior. Nanotechnology 27:195702. https://doi.org/10.1088/0957-4484/27/19/195702
Lopez-Lopez MT, Kuzhir P, Bossis G, Mingalyov P (2008a) Preparation of well-dispersed magnetorheological fluids and effect of dispersion on their magnetorheological properties. Rheol Acta 47:787–796. https://doi.org/10.1007/s00397-008-0271-6
Lopez-Lopez MT, Zugaldia A, Gomez-Ramirez A, Gonzalez-Caballero F, Duran JDG (2008b) Effect of particle aggregation on the magnetic and magnetorheological properties of magnetic suspensions. J Rheol 52:901–912. https://doi.org/10.1122/1.2931008
Machovsky M, Mrlik M, Kuritka I, Pavlinek V, Babayan V (2014) Novel synthesis of core-shell urchin-like ZnO coated carbonyl iron microparticles and their magnetorheological activity. RSC Adv 4:996–1003. https://doi.org/10.1039/c3ra44982c
Machovsky M, Mrlik M, Plachy T, Kuritka I, Pavlinek V, Kozakova Z, Kitano T (2015) The enhanced magnetorheological performance of carbonyl iron suspensions using magnetic Fe_3O_4/ZHS hybrid composite sheets. RSC Adv 5:19213–19219. https://doi.org/10.1039/c4ra14054k
Marins JA, Plachy T, Kuzhir P (2019) Iron-sepiolite magnetorheological fluids with improved performances. J Rheol 63:125–139. https://doi.org/10.1122/1.5048051
Matyjaszewski K (2012) Atom transfer radical polymerization (ATRP): current status and future perspectives. Macromolecules 45:4015–4039. https://doi.org/10.1021/ma3001719
Morillas JR, Bombard AJF, de Vicente J (2018) Magnetorheology of bimodal fluids in the single-multidomain limit. Ind Eng Chem Res 57:13427–13436. https://doi.org/10.1021/acs.iecr.8b03438
Park BJ, Fang FF, Choi HJ (2010) Magnetorheology: materials and application. Soft Matter 6:5246–5253. https://doi.org/10.1039/c0sm00014k
Park DE, Chae HS, Choi HJ, Maity A (2015) Magnetite-polypyrrole core-shell structured microspheres and their dual stimuli-response under electric and magnetic fields. J Mater Chem C 3:3150–3158. https://doi.org/10.1039/c5tc00007f
Park DE, Choi HJ, Vu CM (2016) Stimuli-responsive polyaniline coated silica microspheres and their electrorheology. Smart Mater Struct 25:055020. https://doi.org/10.1088/0964-1726/25/5/055020
Parsian M, Mutlu P, Yalcin S, Tezcaner A, Gunduz U (2016) Half generations magnetic PAMAM dendrimers as an effective system for targeted gemcitabine delivery. Int J Pharm 515:104–113. https://doi.org/10.1016/j.ijpharm.2016.10.015
Plachy T, Kutalkova E, Sedlacik M, Vesel A, Masar M, Kuritka I (2018) Impact of corrosion process of carbonyl iron particles on magnetorheological behavior of their suspensions. J Ind Eng Chem 66:362–369. https://doi.org/10.1016/j.jiec.2018.06.002
Roupec J, Mazurek I (2011) Stability of magnetorheological effect during long term operation. Springer-Verlag, Berlin
Roupec J, Mazurek I, Strecker Z, Klapka M (2013) The behavior of the MR fluid during durability test. In: Unal HI (ed) 13th International Conference on Electrorheological Fluids and Magnetorheological Suspensions, vol 412. Iop Publishing Ltd, Bristol
Sedlacik M, Pavlinek V (2014) A tensiometric study of magnetorheological suspensions' stability. RSC Adv 4:58377–58385. https://doi.org/10.1039/c4ra11842a
Seo YP, Han S, Choi J, Takahara A, Choi HJ, Seo Y (2018) Searching for a stable high-performance magnetorheological suspension. Adv Mater 30:1704769. https://doi.org/10.1002/adma.201704769
Ulicny JC, Balogh MP, Potter NM, Waldo RA (2007) Magnetorheological fluid durability test - iron analysis. Mater SciEng A-Struct

Mater Prop Microstruct Process 443:16–24. https://doi.org/10.1016/j.msea.2006.06.050

Utami D, Ubaidillah MSA, Imaduddin F, Nordin NA, Bahiuddin I, Aziz SAA, Mohamad N, Choi SB (2018) Material characterization of a magnetorheological fluid subjected to long-term operation in damper. Materials 11:2195. https://doi.org/10.3390/ma11112195

Volkova O, Bossis G, Guyot M, Bashtovoi V, Reks A (2000) Magnetorheology of magnetic holes compared to magnetic particles. J Rheol 44:91–104. https://doi.org/10.1122/1.551075

Yang YB, Li L, Chen G (2009) Static yield stress of ferrofluid-based magnetorheological fluids. Rheol Acta 48:457–466. https://doi.org/10.1007/s00397-009-0346-z

Yin JB, Wang XX, Zhao XP (2015) Silicone-grafted carbonaceous nanotubes with enhanced dispersion stability and electrorheological efficiency. Nanotechnology 26:065704. https://doi.org/10.1088/0957-4484/26/6/065704

Zhang P, Dong YZ, Choi HJ, Lee CH (2018) Tribological and rheological tests of core-shell typed carbonyl iron/polystyrene particle-based magnetorheological fluid. J Ind Eng Chem 68:342–349. https://doi.org/10.1016/j.jiec.2018.08.005

Zhu XC, Jing XJ, Cheng L (2012) Magnetorheological fluid dampers: a review on structure design and analysis. J Intell Mater Syst Struct 23:839–873. https://doi.org/10.1177/1045389x12436735